Time-Dependent Density Functional Calculations on the Electronic Absorption Spectra of an Asymmetric Meso-Substituted Porphyrin and Its Zinc Complex

Oana Cramariuc,*,†,‡ Terttu I. Hukka,‡,§ and Tapio T. Rantala†,∥

Institute of Physics, Tampere University of Technology, P.O. Box 692, FIN-33101, Tampere, Finland, and Institute of Materials Chemistry, Tampere University of Technology, P.O. Box 541, FIN-33101, Tampere, Finland

In the present work, the time-dependent density functional theory (TD-DFT) is applied to study the electronic transitions which give rise to the near-ultraviolet−visible (near-UV−vis) optical absorptions of 3,4-dimethyl-*N*-{2-[10,15,20-tris-(3,5-di-*tert*-butyl-phenyl)-porphyrin-5-yl]-phenyl} benzamide (H_2P−O34) and its zinc complex ZnP−O34. Optimizations of the molecular structures were performed using the GGA type Perdew−Burke−Ernzerhof exchange-correlation functional. Excitation energies and oscillator strengths were obtained from the TD-DFT calculations. Calculations were also carried out by using the BP and B3LYP functionals. A large number of electronic transitions are responsible for the optical absorptions in the near-UV−vis region. It was also found that distortions induced to the porphyrin ring by the substituents contribute <10% to the red shifts of the absorption wavelengths of the substituted porphyrins with respect to the unsubstituted porphyrins. The energies of the lowest triplet states were calculated to be 1.44 eV for H_2P−O34 and 1.61 eV for ZnP−O34.

Introduction

The molecular structures and electronic properties of porphyrin−fullerene dyads, in which either H_2P−O34 or its zinc complex ZnP−O34 acts as an electron donating unit, have been studied by various experimental methods during the past years.[1−3] Results from near-ultraviolet−visible (near-UV−vis) absorption spectroscopy and from fluorescence measurements performed by monitoring emission at the Soret band region suggest that a photoinduced electron transfer from the donating unit to the acceptor could lead to a formation of a charge-separated state which lives long enough to allow fabrication of molecular optoelectronic devices.[1] Thus, the theoretical study of the electronic properties and optical absorptions of H_2P−O34 and ZnP−O34 is important for understanding the electron donor characteristics of these molecules.

H_2P−O34 is an asymmetric substituted porphyrin (see Figure 1a), and its experimental near-UV−vis spectrum resembles the spectra of other porphyrins including the unsubstituted porphyrin, that is, porphine (H_2P). In the same way, the absorption spectrum of ZnP−O34 is similar to the spectrum of the unsubstituted zinc porphyrin, that is, zinc porphine (ZnP). The experimental near-UV−vis absorption spectra of porphyrins have four weak absorptions in the visible region, which are called the *Q* band. In addition, there is a very strong absorption band in the near-UV region. This band is called the Soret band or the *B* band. In addition to these, there are some smaller intensity bands at lower wavelengths, namely, the *N*, *L*, and *M* bands.

The peaks of the *Q* band are due to vibronic transitions and are labeled Q_x^0, Q_x^1, Q_y^0, and Q_y^1. The Q_x^0 and Q_y^0 peaks are generally interpreted as pure electronic transitions.[4,5] The absorption spectra of metalloporphyrins and porphyrins differ mainly by the number of absorptions in the *Q* band. There are only two *Q* band transitions in metalloporphyrins, that is, Q^0 and Q^1, out of which Q^1 is vibronic. The absorption spectra of porphine and metal-substituted porphine are usually qualitatively interpreted on the basis of Gouterman's four-orbital model which considers only transitions involving the two highest occupied orbitals and the two lowest unoccupied orbitals.[4−6] Most theoretical calculations are in good agreement with this model, although several papers comment on the necessity of accounting for more transitions involving also lower occupied and higher unoccupied orbitals besides those of the Gouterman's model.[8−10] Actually, also in the appendix of Gouterman's "Part II. Four Orbital Model" article, the need for including more excited states than those of the four-orbital model for a description of the UV absorption, at least, is brought into discussion.[5] Moreover, most theoretical studies have been performed on symmetric D_{2h} and D_{4h} porphyrins which are the ones analyzed also in Gouterman's articles. Asymmetric substitution of the porphyrin ring and drastic lowering of the symmetry of the molecule will result in strong mixing of configurations, and this is an ongoing research field. Experimental results of fluorescence spectroscopy measurements of porphyrins indicate that the *B* band absorption should be described by using a manifold of vibronic levels belonging to two or more electronic states.[7]

Recent time-dependent density functional theory (TD-DFT) calculations on H_2P,[8,11,12] ZnP,[9,13] and some other metalloporphines[9,13] have identified two electronic excitations which give rise to the *B* band. In the cases of H_2P−O34 and ZnP−O34, however, ground state DFT calculations[14] have identified a large number of one-electron transitions between 350 and 450 nm, which have all been assigned to *B* band absorptions. A large number of electronic transitions as well as the large amount of molecular orbitals (MOs) involved in these transitions are
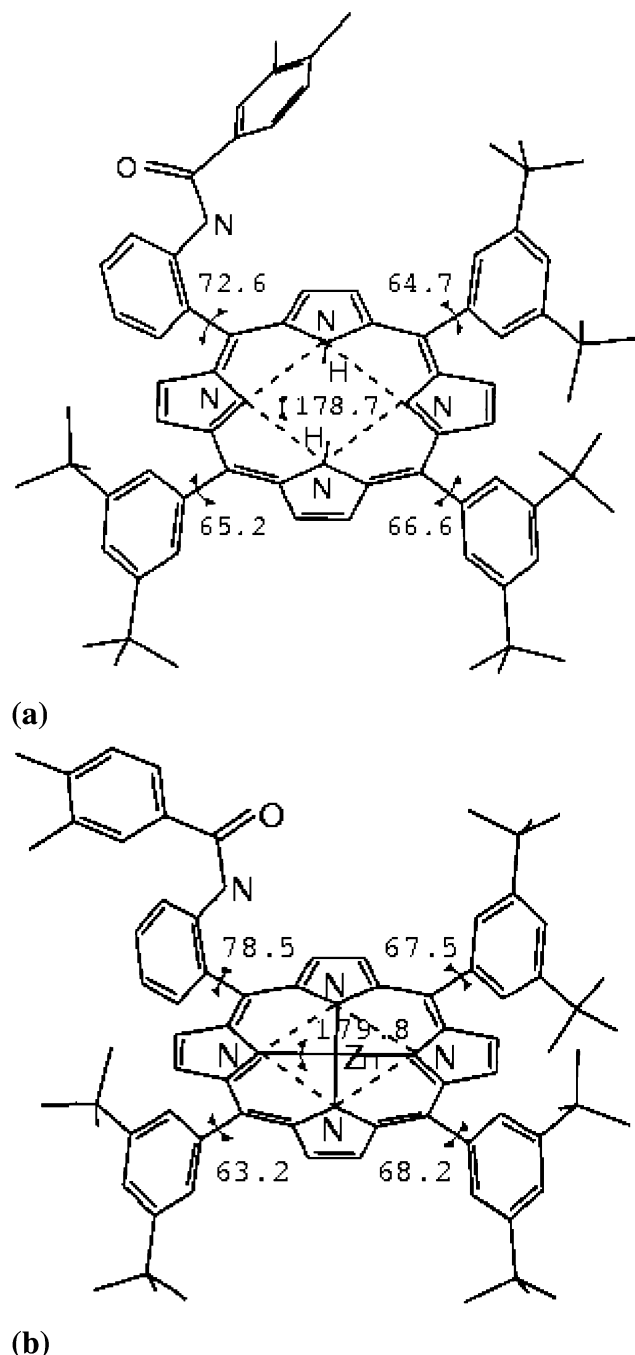
* Corresponding author. E-mail: oana.cramariuc@tut.fi.
† Institute of Physics.
‡ Institute of Materials Chemistry.
§ E-mail: Terttu.Hukka@tut.fi.
∥ E-mail: Tapio.Rantala@tut.fi.

(a)

(b)

Figure 1. Optimized molecular structures of (a) H_2P-O34 and (b) $ZnP-O34$. The hydrogen atoms have been omitted except from the nitrogen atoms of the pyrrole rings. The numbers in the figure represent the values of the dihedral angles, in degrees, between the phenyl rings and the porphyrin ring.

attributed to complex electronic structures and the lowest symmetry, that is, C_1, of these molecules.[14]

In the present work, we have used the TD-DFT to determine the electronic excitations which correspond to the experimental near-UV−vis absorptions of H_2P-O34 and $ZnP-O34$ molecules. Red shifts of the near-UV−vis absorption peaks have been investigated in the light of electronic effects of the substituents at the porphyrin ring and of distortions in the porphyrin ring caused by the substituents. The relative contributions of these two factors are determined. We have also evaluated the lowest triplet state energies. The triplet states are usually long living due to the selection rules and are, therefore, relevant to molecular electronics as well.

Computational Methods

Geometry optimizations, electronic structure investigations, and TD-DFT calculations were performed using two different generalized-gradient approximation (GGA) exchange-correlation functionals, that is, the Perdew−Burke−Ernzerhof (PBE)[15−18] and Becke−Perdew (BP) functionals.[17−21] In addition, a hybrid functional, that is, the Becke3LYP (B3LYP) functional, was used.[17−20,22,23] The PBE functional is a reformulation of the first-principles GGA functional PW91. On one hand, it is a simplification, but on the other hand, it is an improvement on PW91. These two functionals have been found to yield essentially the same results for atomic energetics, with PBE being only slightly more accurate than PW91.[15] Therefore, PBE is not expected to differ from PW91, at least not when describing porphyrin in its singlet ground state. The BP functional has become popular, and it has also been successfully used in the TD-DFT calculations of the absorption spectra of porphine and magnesium porphine.[8,9] To find a general view of different functionals, we have carried out calculations also using the popular B3LYP functional that involves semiempirical parameters and which was also used in TD-DFT calculations of the absorption spectra of porphine and metalloporphines.[8,9,11−13]

The Karlsruhe split-valence basis set augmented[24] with polarization functions (SVP)[25] was used. The SVP basis set consists of two basis functions for H (4s)/[2s], six basis functions for C (7s4p1d)/[3s2p1d], and six basis functions for N (7s4p1d)/[3s2p1d]. The terms in parentheses represent the numbers of primitive functions of each type, and the terms in brackets represent the numbers of contracted basis functions of each type. The resolution of identity approach (RI) was used together with the PBE and BP functionals to reduce the computational effort and, accordingly, the time needed for calculations.[26]

The excitation energies and the oscillator strengths were obtained from the TD-DFT calculations. Also, the energies of the lowest triplet states of H_2P-O34 and $ZnP-O34$ were calculated by using the same method. The first step of the TD-DFT calculation employs a self-consistent ground state Kohn−Sham (KS) computation.[27] The second step consists of solving the central equation of the TD-DFT response theory by using the adiabatic local density approximation (ALDA) for the functional derivatives of the exchange-correlation potential.[27] All calculations were performed with the Turbomole software package.[28]

Results

Geometries and Electronic Structures of H_2P-O34 and $ZnP-O34$. The DFT-optimized geometries of H_2P-O34 and $ZnP-O34$ are drawn in parts a and b of Figure 1, respectively. Some bond lengths and bond angles are listed in Table 1, for H_2P-O34, and in Table 2, for $ZnP-O34$. Also the bond lengths and bond angles from our previous DFT/PW91 calculations are given in Tables 1 and 2.[14] The complete sets of Cartesian coordinates are available upon request. Both molecules adopt a slightly nonplanar geometry with the lowest symmetry. Essentially the same structures are obtained from the DFT calculations performed with different functionals (see Tables 1 and 2). For both porphyrin molecules, that is, H_2P-O34 and $ZnP-O34$, the differences in bond lengths are $\leq 2 \times 10^{-3}$ Å and those in bond angles $\leq 0.2°$. The B3LYP functional, which was used for the calculations of H_2P-O34 (see Table 1) yields only slightly larger values than the GGA functionals. To our knowledge, no experimental data are available in the literature on the structural parameters presented in Tables 1 and 2.

TABLE 1: Some Calculated Bond Lengths (Å) and Bond Angles (deg) in H$_2$P−O34

structural parameters	PBE/SVP	BP/SVP	PW91/DNP[12]	B3LYP
		Bond Lengths (Å)		
H−N	1.029−1.031	1.030	1.026	1.020
N−C$_\alpha$	1.380−1.381	1.381−1.383	1.377−1.379	1.383−1.385
(N−C$_\alpha$)^a	1.370−1.372	1.372−1.374	1.371−1.372	1.370−1.372
C$_\beta$−C$_\alpha$	1.441−1.442	1.441−1.442	1.432−1.434	1.443−1.446
(C$_\beta$−C$_\alpha$)^a	1.465−1.466	1.465−1.467	1.457−1.458	1.469−1.470
C$_\beta$−C$_\beta$	1.380−1.381	1.381−1.382	1.373−1.376	1.380−1.381
(C$_\beta$−C$_\beta$)^a	1.366−1.367	1.367	1.358−1.359	1.366
C$_m$−C$_\alpha$	1.415−1.416	1.414−1.415	1.407−1.409	1.410−1.414
(C$_m$−C$_\alpha$)^a	1.420−1.423	1.422−1.424	1.414−1.415	1.418−1.421
C$_\beta$−H	1.095−1.096	1.095−1.096	1.086−1.088	1.087−1.088
(C$_\beta$−H)^a	1.096−1.097	1.097	1.086−1.087	1.088
		Bond Angles (deg)		
H−N−C$_\alpha$	124.3−125.0	124.2−125.3	126.4−126.8	124.1−124.9
C$_\alpha$−N−C$_\alpha$	110.6−110.7	110.5−110.7	110.7−110.8	110.7−110.8
(C$_\alpha$−N−C$_\alpha$)^a	105.4−105.5	105.3−105.4	105.4	108.1−108.2
N−C$_\alpha$−C$_\beta$	106.6−106.8	106.6−106.8	106.4−106.5	106.3−106.5
(N−C$_\alpha$−C$_\beta$)^a	111.1−111.2	111.0−111.4	110.9	110.5−110.7
C$_\alpha$−C$_\beta$−C$_\beta$	108.0	107.9−108.1	108.1−108.2	108.2
(C$_\alpha$−C$_\beta$−C$_\beta$)^a	106.2	106.1−106.2	106.3−106.5	106.3−106.4
C$_\alpha$−C$_m$−C$_\alpha$	124.9−125.4	124.8−125.5	125.0−125.7	124.7−125.3

^{a} Pyrrole rings in which the nitrogen atoms are unprotonated.

TABLE 2: Some Calculated Bond Lengths (Å) and Bond Angles (deg) in ZnP−O34

structural parameters	PBE/SVP	BP/SVP	PW91/DNP
		Bond Lengths (Å)	
Zn−N	2.062−2.065	2.061−1.063	2.059−2.060
N−C$_\alpha$	1.379−1.381	2.380−2.383	1.378−1.379
C$_\beta$−C$_\alpha$	1.451−1.453	2.452−1.453	1.443−1.444
C$_\beta$−C$_\beta$	1.373−1.375	1.374−1.375	1.365−1.357
C$_m$−C$_\alpha$	1.416−1.418	1.417−1.419	1.412−1.413
C$_\beta$−H	1.096−1.098	1.096−1.098	1.086−1.088
		Bond Angles (deg)	
N−Zn−N	89.8−90.3	89.9−90.1	89.8−90.1
C$_\alpha$−N−C$_\alpha$	106.8	106.7−106.8	106.9−107.0
N−C$_\alpha$−C$_\beta$	109.6−109.8	109.7−109.8	109.3−109.5
C$_\alpha$−C$_\beta$−C$_\beta$	106.7−107.0	106.8−106.9	107.1−107.2
C$_\alpha$−C$_m$−C$_\alpha$	124.8−124.9	124.8−124.9	124.9−125.0
Zn−N−C$_\alpha$	125.7−126.1	126.5−126.7	125.9−126.0

The energies of some frontier MOs of H$_2$P−O34 and ZnP−O34 are given in Table 3. The energies of the MOs calculated with the PBE functional are slightly higher than those calculated with the BP functional. However, the energies calculated using the highest occupied molecular orbital (HOMO) energy as a reference (ϵ) differ only in the second decimal for the PBE and BP functionals. The DFT/PBE calculations on H$_2$P−O34 yield a gap of 1.70 eV between the highest occupied molecular orbital (HOMO) and the lowest unoccupied molecular orbital (LUMO). The HOMO−LUMO energy gap obtained with the hybrid functional is almost 1 eV larger. In the case of ZnP−O34, the PBE functional yields 1.83 eV for the HOMO−LUMO gap.

Near-UV−vis Absorption Spectra. Because no experimental gas phase absorption spectra have been found in the literature for H$_2$P−O34 and ZnP−O34, the liquid phase data are used when the calculated absorption spectra are compared with experimental results. The experimental absorption spectra of H$_2$P−O34 and ZnP−O34 were measured in benzene.[1−3]

H$_2$P−O34. The wavelengths and oscillator strengths of the TD-DFT/PBE-calculated excitations, which can be assigned to the Q and B bands, are listed in Table 4. The weights of the one-electron transitions contributing more than 5% to the excitations are also given in Table 4. Several other excitations

TABLE 3: Calculated Energies of the Frontier Molecular Orbitals of H$_2$P−O34 and ZnP−O34 Using the HOMO Energy as a Reference (ϵ)^a

molecular orbitals	H$_2$P−O34			ZnP−O34	
	PBE ϵ (eV)	BP ϵ (eV)	B3LYP ϵ (eV)	PBE ϵ (eV)	BP ϵ (eV)
LUMO + 7	3.64	3.64	4.97	3.68	3.62
LUMO + 6	3.56	3.58	4.86	3.63	3.56
LUMO + 5	3.51	3.54	4.81	3.62	3.63
LUMO + 4	3.48	3.50	4.78	3.46	3.45
LUMO + 3	2.96	2.99	4.20	3.06	3.10
LUMO + 2	2.78	2.79	3.98	2.91	2.93
LUMO + 1	1.73	1.75	2.68	1.85	1.87
LUMO	1.70	1.72	2.64	1.83	1.84
HOMO	0	0	0	0	0
HOMO − 1	−0.41	−0.38	−0.40	−0.29	−0.28
HOMO − 2	−0.52	−0.46	−0.76	−0.57	−0.60
HOMO − 3	−0.84	−0.86	−1.31	−0.70	−0.74
HOMO − 4	−0.96	−0.94	−1.47	−0.71	−0.83
HOMO − 5	−1.02	−1.00	−1.52	−1.02	−0.98
HOMO − 6	−1.17	−1.14	−1.53	−1.07	−1.13
HOMO − 7	−1.22	−1.19	−1.55	−1.09	−1.16

^{a} The HOMO energies of H$_2$P−O34 are −4.68, −4.78, and −5.08 eV for PBE, BP, and B3LYP, respectively. The HOMO energies of ZnP−O34 are −4.71 and −4.79 eV for PBE and BP, respectively.

with wavelengths below the considered near-UV−vis interval were obtained from the TD-DFT calculations. These can be most probably correlated to the lower wavelength absorption bands of porphyrins, although they have slightly larger oscillator strengths than what should be expected. The experimental wavelengths and the absorbances of the liquid phase near-UV−vis absorption spectrum are also given in Table 4. In addition, the calculated electronic transition energies are presented in Figure 2a with a 6 nm broadening of Gaussian line shape, to simulate the experimental spectra as well as the vibrational broadening that is not included in our present calculations. In Figure 2, the areas under the calculated and experimental spectra were normalized to 1.

The calculated electronic excitations at 631.6 and 598.8 nm compare well with the experimental wavelengths of the absorption maxima of the Q_x^0 and Q_y^0 peaks, that is, 648.0 and 552.0 nm, respectively (see Table 4 and Figure 2). Moreover, in the

TABLE 4: TD-DFT/PBE-Calculated and Experimental Wavelengths (nm, eV), the Corresponding One-Electron Transitions, and Oscillator Strengths of the Electronic Transitions of H_2P-O34[a]

|		TD-DFT/PBE				experimental		
	excitation (nm)	excitation (eV)	one-electron transition	weight (%)	oscillator strength	excitation (nm)	excitation (eV)	absorbance
Q_x^0	631.6	1.96	$H \rightarrow L+1$; $H \rightarrow L$	42.9; 29.0	0.043	648.0	1.91	0.015
			$H-1 \rightarrow L$; $H-1 \rightarrow L+1$	16.4; 9.9				
Q_y^0	598.8	2.07	$H \rightarrow L$; $H \rightarrow L+1$	41.4; 27.4	0.068	552.0	2.25	0.039
			$H-1 \rightarrow L+1$; $H-1 \rightarrow L$	14.7; 9.3				
B	447.7	2.77	$H-4 \rightarrow L+2$; $H-5 \rightarrow L$	30.3; 18.3	0.191	423.0	2.93	2.319
			$H-1 \rightarrow L$; $H-5 \rightarrow L+1$;	15.6; 15.0; 6.2				
			$H-1 \rightarrow L+1$					
B	445.8	2.78	$H-4 \rightarrow L$; $H-4 \rightarrow L+1$	58.8; 37.1	0.003			
B	444.5	2.79	$H \rightarrow L+2$; $H-5 \rightarrow L$;	67.5; 14.6; 7.3	0.032			
			$H-5 \rightarrow L+1$					
B	440.0	2.80	$H-5 \rightarrow L$; $H-5 \rightarrow L+1$	40.3; 23.1	0.057			
			$H-4 \rightarrow L+1$; $H-4 \rightarrow L$	14.2; 6.9				
B	438.4	2.82	$H-4 \rightarrow L+1$; $H-4 \rightarrow L$	42.8; 29.5	0.018			
			$H-5 \rightarrow L+1$; $H-5 \rightarrow L$	11.5; 6.6				
B	431.5	2.87	$H-1 \rightarrow L+1$; $H \rightarrow L$	29.6; 8.7	0.428			
			$H-11 \rightarrow L+1$; $H-5 \rightarrow L$	8.6; 6.8				
			$H-6 \rightarrow L+1$; $H-6 \rightarrow L$	5.7; 5.5				
B	428.7	2.89	$H-6 \rightarrow L$; $H-5 \rightarrow L+1$	64.3; 9.4	0.096			
B	426.5	2.90	$H-6 \rightarrow L$; $H-5 \rightarrow L+1$	23.2; 15.5	0.264			
			$H-1 \rightarrow L$; $H-11 \rightarrow L$	10.2; 10.1				
			$H-6 \rightarrow L+1$; $H-7 \rightarrow L$	8.9; 8.8				
B	421.3	2.94	$H-6 \rightarrow L+1$; $H-7 \rightarrow L$;	53.9; 23.8; 5.5	0.012			
			$H \rightarrow L+3$					
B	419.9	2.05	$H-7 \rightarrow L$; $H-6 \rightarrow L+1$;	59.6; 13.0; 5.4	0.134			
			$H-5 \rightarrow L+1$					
B	418.7	2.96	$H-8 \rightarrow L$	82.1	0.023			
B	416.1	2.98	$H-9 \rightarrow L$; $H-7 \rightarrow L+1$;	40.0; 29.8; 26.0	0.012			
			$H-10 \rightarrow L$					
B	415.4	2.98	$H-7 \rightarrow L+1$; $H-9 \rightarrow L+1$	51.2; 22.6	0.016			
			$H-10 \rightarrow L+1$; $H-12 \rightarrow L+1$	8.1; 6.8				
B	413.9	2.99	$H-8 \rightarrow L+1$	92.3	0.003			
B	412.0	3.01	$H-9 \rightarrow L+1$; $H-10 \rightarrow L+1$	64.9; 21.5	0.006			
B	410.9	3.02	$H-11 \rightarrow L$; $H-10 \rightarrow L$	36.1; 24.0	0.036			
			$H-10 \rightarrow L+1$; $H-9 \rightarrow L$;	15.9; 7.2; 6.0				
			$H-11 \rightarrow L+1$					
B	409.7	3.03	$H-10 \rightarrow L+1$; $H-10 \rightarrow L$	20.2; 19.7	0.054			
			$H-11 \rightarrow L+1$; $H-11 \rightarrow L$;	17.2; 13.7; 12.3				
			$H-9 \rightarrow L$					
B	406.8	3.05	$H-10 \rightarrow L+1$; $H-12 \rightarrow L$	23.3; 22.8	0.014			
			$H-12 \rightarrow L+1$; $H-11 \rightarrow L$;	14.3; 10.7; 7.4				
			$H-9 \rightarrow L+1$					
B	405.8	3.06	$H-12 \rightarrow L$; $H-11 \rightarrow L+1$;	36.7; 25.1; 23.7	0.029			
			$H-12 \rightarrow L+1$					
B	403.2	3.07	$H-11 \rightarrow L+1$; $H-12 \rightarrow L$	30.0; 12.9	0.121			
			$H-14 \rightarrow L$; $H-13 \rightarrow L$	11.0; 10.0				
			$H-10 \rightarrow L+1$; $H-16 \rightarrow L$;	7.0; 6.3; 6.0				
			$H-9 \rightarrow L+1$					
B	400.8	3.09	$H-12 \rightarrow L+1$; $H-14 \rightarrow L+1$	44.3; 10.8	0.058			
			$H-13 \rightarrow L+1$; $H-12 \rightarrow L$	8.5; 7.0				

[a] Excitation weights which are smaller than 5% have been neglected.

visible part of the spectrum, the number of the calculated excitations is very similar to that obtained by the TD-DFT calculations with H_2P.[8,11,12,14] The calculated excitations at 556.9, 549.9, 489.7, and 483.9 nm are not given in Table 4 because (1) their oscillator strengths are only ~10^{-3}, which is an order of magnitude smaller than the transitions giving rise to the Q_x^0 and Q_y^0 peaks and (2) there are no experimental absorptions which could be related to these excitations. It is also possible that these excitations are not resolved in the experimental spectrum.

All the 21 calculated electronic excitations between 447.7 and 400.8 nm can be assigned to the B band. The absorption of the experimentally measured B band covers a spectral region of ~450.0−400.0 nm. The large amount of excitations in the B band region can only be explained by electronic transitions taking place between a large number of occupied and unoc-cupied orbitals. Inspection of Table 4 reveals that the electronic excitations, which give rise to the B band, involve transitions between 17 occupied and 3 unoccupied MOs. The large number of transitions, which involve a large number of MOs, can be mainly attributed to two factors. First, H_2P-O34 belongs to the lowest symmetry point group, that is, C_1. Therefore, no symmetry restrictions apply to the electronic transitions; that is, from the symmetry point of view, all transitions are allowed and, therefore, a number of almost forbidden transitions emerge with weak intensities. Second, the occupied MOs, which locate below HOMO − 1, are quite close in energy; for example, the energy difference between HOMO − 1 and HOMO − 16 is only 1 eV (see Table 3).

The TD-DFT calculations with two different GGA function-als, PBE and BP, yield essentially the same results. Both func-
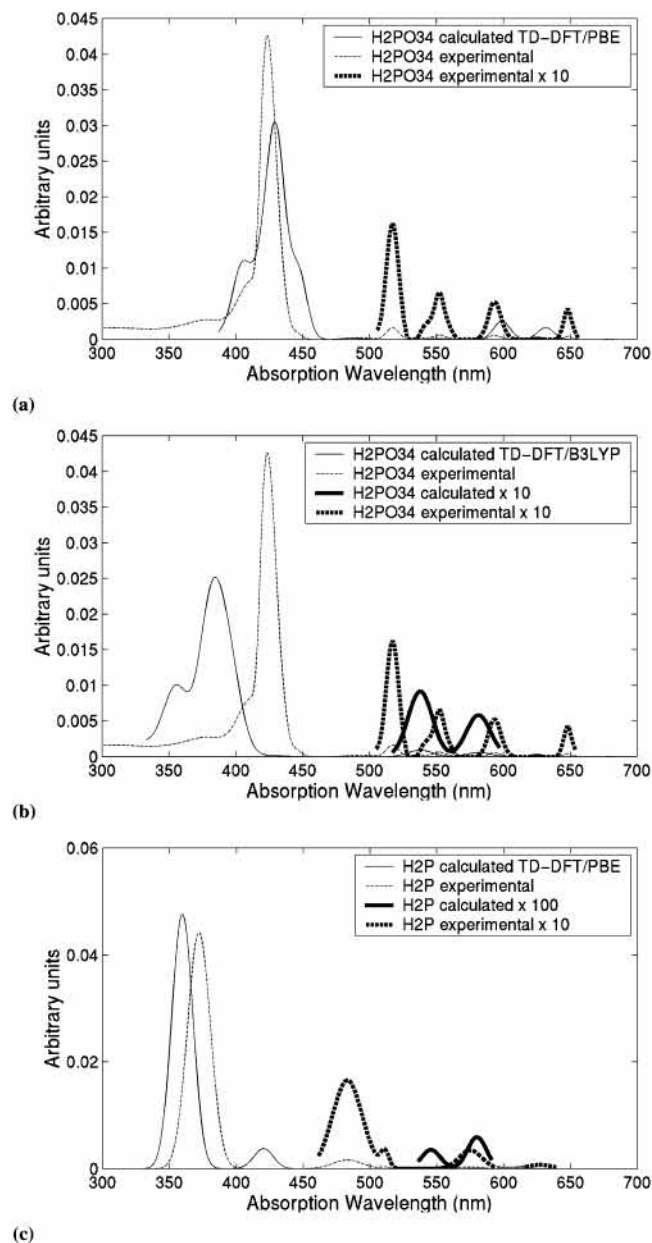
Figure 2. Calculated (solid line) and experimental (dotted line) absorption spectra of (a and b) H$_2$P—O34 and (c) H$_2$P.[14] Calculated plots are presented with a 6 nm broadening of Gaussian line shape. The areas under the plots are normalized to 1. The thick lines are drawn after multiplication of the *y*-values corresponding to the visible wavelength region. The multiplication factors are given in the legends of the plots. The experimental gas phase absorption spectrum of H$_2$P was drawn after the experimental data provided in ref 32.

tionals yield almost the same excitation wavelengths and oscillator strengths. However, there are differences between the excitation weights and the MOs involved in one-electron transitions. The differences are larger for the *B* band excitations than for the *Q* band excitations. In the *Q* band excitations, the differences are restricted to the LUMO and LUMO + 1 orbitals. These orbitals are interchanged if the TD-DFT/BP results are compared to the TD-DFT/PBE results. These differences originate from small differences in structures, which are obtained with the PBE and BP functionals (see Table 1). The TD-DFT/PBE calculations, which we have carried out by using the DFT/BP-optimized geometries, yield practically the same excitation wavelengths, oscillator strengths, excitation weights, and MOs involved in one-electron transitions as the TD-DFT/BP calculations.

The TD-DFT/B3LYP-calculated excitations above 330 nm are given in Table 5 and Figure 2b. In addition, the one-electron transitions contributing more than 5% as well as their weights, which are indicated in percents, are given in Table 5. Examination of the spectra in Figure 2 and the numerical data in Tables 4 and 5 reveals several differences between the results calculated with the GGA type and hybrid functionals. First, the absorption spectrum calculated with B3LYP is shifted toward higher wavelengths as compared to the PBE absorption spectrum. Second, the number of excitations which give rise to the *B* band is smaller in the B3LYP-calculated spectrum. The difference in the number of excitations would be even larger if we did not consider those excitations which have oscillator strengths smaller than 10^{-2} and are therefore 2 orders of magnitude smaller than the strongest excitation of the *B* band. The different results obtained with the GGA and hybrid functionals can be related to the sensitivity of the TD-DFT calculations to the asymptotic decay of the exchange-correlation potential.[27,29] This in turn influences the quality of the orbital energy differences which enter the TD-DFT formalism as a first approximation to the excitation energies.[27,29] As can be seen from Table 3, there are differences of almost 1 eV between the orbital energy differences calculated with the GGA and hybrid functionals. It could be expected that hybrid functionals, which in general exhibit an improved asymptotic decay of the exchange-correlation potential over the GGA functionals, yield more correct excitation energies. However, the hybrid functionals are improved by mixing of exact Hartree—Fock exchange with semilocal functionals, and as pointed out in ref 30, the optimum amount of mixing is far from universal. On the other hand, the PW91 functional and its modified form, the PBE functional, are derived without semiempirical parameters. Therefore, answering the question of whether the GGA functionals or the hybrid functionals can be trusted more is not straightforward. While the search for improved functionals is continuing, discussions on the influences of the most widely used functionals on the TD-DFT results can be found in several articles and books.[27,29]

When comparing the optical absorptions of H$_2$P—O34 with those of H$_2$P,[14] one can find differences not only in the number of electronic excitations which contribute to the *B* band absorptions, as explained in the Introduction, but also in the excitation wavelengths of the *B* and *Q* bands. Both the experimental and calculated excitation wavelengths of H$_2$P—O34 are shifted toward red when compared to H$_2$P (see Figure 2). In the experimental absorption spectra, the red shifts are ∼30 nm. The TD-DFT-calculated red shifts of the *Q* and *B* bands of H$_2$P—O34 with respect to H$_2$P are ∼53.0 and ∼11.0 nm, respectively.

Red shifts are due to the electronic effects of the substituents as well as to the geometrical distortions of the porphyrin ring caused by the substituents, that is, nonplanarity and changes of bond lengths and bond angles. To quantify the total contribution of the geometrical changes alone, we have carried out TD-DFT/PBE calculations also for a modified H$_2$P—O34 (m—H$_2$P—O34) molecule in which all the substituents were replaced by hydrogens while retaining the distorted porphyrin skeleton. The geometrical distortions of the porphyrin ring contribute ∼10% to the red shifts of the absorption peaks. The red shifts of the *Q* and *B* bands of m—H$_2$P—O34 with respect to H$_2$P are ∼5.0 and ∼1.0 nm, respectively.

ZnP—O34. The TD-DFT/PBE-calculated and experimental spectra of ZnP—O34 are presented in Figure 3a. A 6 nm broadening with Gaussian line shape was applied to the calculated electronic excitations. Inspection of Figure 3a reveals

TABLE 5: TD-DFT/B3LYP-Calculated and Experimental Wavelengths (nm, eV), the Corresponding One-Electron Transitions, and Oscillator Strengths of the Electronic Transitions of H_2P-O34[a]

	TD-DFT/B3LYP				experimental			
	excitation (nm)	excitation (eV)	one-electron transition	weight (%)	oscillator strength	excitation (nm)	excitation (eV)	absorbance
Q_x^0	581.3	2.13	$H \rightarrow L$; $H-1 \rightarrow L+1$	56.7; 23.7	0.039	648.0	1.91	0.015
			$H \rightarrow L+1$	12.8				
Q_y^0	537.7	2.30	$H \rightarrow L+1$; $H-1 \rightarrow L$	53.4; 27.4	0.062	552.0	2.25	0.039
			$H \rightarrow L$	12.8				
B	431.7	2.87	$H-2 \rightarrow L$	94.5	0.007	423.0	2.93	2.319
B	416.1	2.98	$H-2 \rightarrow L+2$	95.3	0.007			
B	394.9	3.14	$H-1 \rightarrow L+1$; $H \rightarrow L$	41.2; 13.6	0.779			
			$H-4 \rightarrow L$; $H-1 \rightarrow L$	13.1; 12.4				
B	381.4	3.25	$H-1 \rightarrow L$; $H \rightarrow L+1$	44.6; 22.4	1.381			
			$H-1 \rightarrow L+1$; $H \rightarrow L$	14.4; 6.6				
	378.5	3.27	$H-3 \rightarrow L$; $H-3 \rightarrow L+1$					
B	356.3	3.48	$H-3 \rightarrow L+1$; $H-4 \rightarrow L$; $H-3 \rightarrow L$	49.2; 26.8; 15.6	0.160			
B	355.3	3.49	$H-4 \rightarrow L$; $H-3 \rightarrow L+1$	46.4; 32.4	0.389			
B	351.3	3.53	$H-4 \rightarrow L+1$; $H-4 \rightarrow L$	87.4; 5.0	0.100			
B	349.0	3.55	$H \rightarrow L+2$	97.6	0.022			
B	341.6	3.63	$H-5 \rightarrow L$; $H-6 \rightarrow L$	85.9; 5.1	0.003			
B	340.2	3.64	$H-5 \rightarrow L+1$; $H-6 \rightarrow L+1$	83.3; 5.0	0.005			
B	337.2	3.68	$H-6 \rightarrow L$; $H-6 \rightarrow L+1$; $H-7 \rightarrow L$	67.5; 12.2; 6.4	0.008			
B	335.0	3.70	$H-7 \rightarrow L$; $H-7 \rightarrow L+1$	51.7; 14.1	0.008			
			$H-10 \rightarrow L$; $H-6 \rightarrow L$	11.6; 7.6				
B	333.8	3.71	$H-7 \rightarrow L+1$; $H-10 \rightarrow L$	49.9; 19.2	0.002			
			$H \rightarrow L+3$; $H-6 \rightarrow L+1$	7.8; 7.1				
B	333.1	3.72	$H-6 \rightarrow L+1$; $H-9 \rightarrow L$	48.0; 14.4	0.007			
			$H-7 \rightarrow L+1$; $H-9 \rightarrow L+1$	8.8; 8.2				
			$H-10 \rightarrow L+1$	6.2				
B	331.4	3.74	$H-9 \rightarrow L+1$; $H-10 \rightarrow L$	29.2; 20.6	0.005			
			$H-7 \rightarrow L$; $H-6 \rightarrow L+1$	14.3; 9.3				
			$H \rightarrow L+3$; $H-9 \rightarrow L$	7.8; 5.7				
B	330.8	3.75	$H-10 \rightarrow L$; $H-9 \rightarrow L+1$	41.2; 27.4	0.054			
			$H \rightarrow L+3$; $H-9 \rightarrow L$	19.1; 12.0				

[a] Excitation weights which are smaller than 5% have been neglected.

that the calculated excitations at 586.8 and 584.9 nm with oscillator strengths of 0.031 and 0.038 can both be assigned to the Q^0 peak, whose maximum appears at 604.0 nm in the experimental spectrum. The maximum absorbance of the Q^0 peak is 0.056. Following are six excitations at 514.5, 511.5, 487.7, 484.8, 483.0, and 480.3 nm which are not visible in Figure 3a because of their very low oscillator strengths. There are no corresponding experimental absorption peaks for these transitions. As in the case of H_2P-O34, these excitations might not be resolved in the experimental spectrum, because of their low oscillator strengths. Subsequent calculated electronic excitations, which start at 433.7 nm, are assigned to the B band. There are 11 electronic excitations in the spectral region of $\sim$430–405 nm. The experimental B band extends from $\sim$440 to $\sim$400 nm. A maximum oscillator strength value of 0.352 was calculated for the excitation at 432.7 nm. This again compares very well with the experimental spectrum in which the B band maximum locates at 432.0 nm and has a maximum absorbance of 1.652.

In a similar manner as in the case of H_2P-O34 above, the electronic excitations of $ZnP-O34$, which give rise to the B band, involve one-electron transitions between a large number of occupied and unoccupied MOs. The excitations which correspond to the Q^0 peak consist of one-electron transitions from HOMO and HOMO $-$ 1 to LUMO and LUMO $+$ 1. The Q^0 peak of ZnP consists of similar one-electron transitions; however, in this case, the LUMO and LUMO $+$ 1 orbitals are degenerate and the HOMO and HOMO $-$ 1 orbitals are nearly degenerate.[14] In the case of $ZnP-O34$, the LUMO and LUMO $+$ 1 orbitals are almost degenerate but the energy difference between HOMO and HOMO $-$ 1 is $\sim$0.3 eV (see Table 3). Therefore, the two one-electron transitions contributing to the

Q^0 peak have slightly different energies, which result in two distinct but energetically close excitations. The electronic excitations, which give rise to the B band, involve transitions between a large number of occupied and unoccupied MOs. The same reasoning as that described above for H_2P-O34 can be also applied for understanding the large number of MOs involved in the electronic transitions of $ZnP-O34$. The TD-DFT results obtained by the PBE and BP functionals yield essentially similar results for the excitation wavelengths and oscillator strengths, but the excitation weights and MOs differ.

Red shifts are also observed when comparing the optical absorptions of $ZnP-O34$ and ZnP (see parts a and b of Figure 3, respectively). As shown above for H_2P-O34 and H_2P and also in the case of their zinc complexes, the experimentally observed red shifts are reproduced by the calculated electronic transitions. The contribution of the geometrical changes to the red shifts was evaluated by calculating the electronic excitations of a modified $ZnP-O34$ (m-$ZnP-O34$) molecule in which all the substituents on the porphyrin ring were replaced by hydrogens. The red shifts (a) of the Q and B bands of $ZnP-O34$ with respect to ZnP are $\sim$55.7 and $\sim$44.0 nm, respectively.[13] The red shifts (b) of the Q and B bands of m-$ZnP-O34$ with respect to ZnP are $\sim$4.5 and $\sim$1.3 nm, respectively.[13] Therefore, the geometrical distortions of the porphyrin ring contribute <8% to the red shifts of the absorption peaks.

Triplet States. Some of the energies of the triplet excited states of H_2P-O34 and $ZnP-O34$ with respect to the ground states are given in Table 6. The calculated energies of the lowest triplet excited states of H_2P-O34 and $ZnP-O34$ are 1.44 and 1.61 eV, respectively. The experimentally obtained values for almost identical porphyrin and zinc porphyrin molecules are 1.40 and 1.64 eV, respectively.[31] The PBE and BP functionals

Electronic Absorption Spectra of H₂P−O34 and ZnP−O34

J. Phys. Chem. A, Vol. 108, No. 43, 2004 **9441**
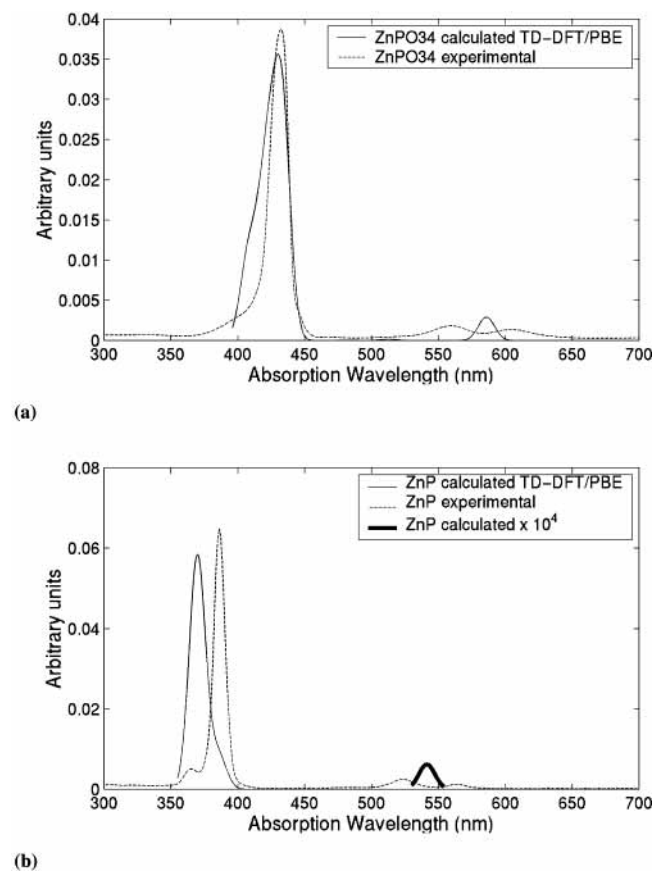
Figure 3. Calculated (solid line) and experimental (dotted line) absorption spectra of (a) ZnP−O34 and (b) ZnP. Calculated plots are presented with a 6 nm broadening of Gaussian line shape. The areas under the plots are normalized to 1. In part b, the thick full line is drawn after multiplication of the *y*-values by 10^4. The experimental gas phase absorption spectrum of ZnP was drawn after the experimental data provided in ref 33.

TABLE 6: TD-DFT/PBE-Calculated Triplet State Energies (eV) of H₂P−O34 and ZnP−O34

H₂P−O34		ZnP−O34	
state	energy (eV)	state	energy (eV)
³A	1.44	³A	1.61
³A	1.56	³A	1.63
³A	1.95	³A	1.98
³A	2.00	³A	2.00
³A	2.20	³A	2.40
³A	2.23	³A	2.42
³A	2.48	³A	2.49
³A	2.53	³A	2.50

yield energies which are the same within 0.03 eV for the eight lowest triplet excited states.

Conclusions

In this work, the TD-DFT was applied to study two asymmetric substituted porphyrins, that is, H₂P−O34 and ZnP−O34, using the PBE and BP functionals of GGA type and the B3LYP hybrid functional.

It was shown that although there are differences between the TD-DFT results obtained with different functionals all calculations support the fact that the *B* band is a result of several electronic excitations which involve a large number of MOs, whereas the peaks in the *Q* band originate from transitions involving only HOMO − 1, HOMO, LUMO, and LUMO + 1. The low symmetry of these porphyrin molecules and the very close spacing of a large number of occupied MOs are two of the factors which contribute to the complex structure of the *B* band. The present results support the results obtained from our previous ground state DFT calculations.[14] The red shifts of the near-UV−vis absorption peaks have been evaluated, and our calculations predict that the contribution of the porphyrin ring distortion is <10% for both substituted porphyrins. The calculated lowest triplet state energies are 1.44 eV for H₂P−O34 and 1.61 eV for ZnP−O34.

References and Notes

(1) Imahori, H.; Akiyama, T.; Taniguchi, S.; Okada, T.; Shirakawa, M.; Sakata, Y. *J. Am. Chem. Soc.* **1996**, *118*, 11771.

(2) Vehmanen, V.; Tkachenko, N. V.; Imahori, H.; Fukuzumi, S.; Lemmetyinen, H. *Spectrochim. Acta, Part A* **2001**, *57*, 2229.

(3) Imahori, N.; Tkachenko, N. V.; Tamaki, K.; Lemmetyinen, H.; Sakata, Y.; Fukuzumi, S. *J. Phys. Chem. A* **2001**, *105*, 1750.

(4) Gouterman, M. *J. Mol. Spectrosc.* **1961**, *6*, 138.

(5) Gouterman, M.; Wagniére, G. H. *J. Mol. Spectrosc.* **1963**, *11*, 108.

(6) Gouterman, M. *J. Chem. Phys.* **1959**, *30*, 1139.

(7) Gurzadyan, G. G.; Tran-Thi, T. H.; Gustavsson, T. *J. Chem. Phys.* **1998**, *108*, 385.

(8) Sundholm, D. *Phys. Chem. Chem. Phys.* **2000**, *2*, 2275.

(9) Sundholm, D. *Chem. Phys. Lett.* **2000**, *317*, 392.

(10) Baraldi, I.; Carnevali, A.; Ponterini, G.; Vanossi, D. *THEOCHEM* **1995**, *333*, 121.

(11) Nguyen, K. A.; Day, P. N.; Pachter, R. *J. Phys. Chem. A* **2000**, *104*, 4748.

(12) van Gisberg, S. J. A.; Rosa, A.; Ricciardi, G.; Baerends, E. J. *J. Chem. Phys.* **1999**, *111*, 2499.

(13) Nguyen, K. A.; Pachter, R. *J. Chem. Phys.* **2001**, *114*, 10757.

(14) Cramariuc, O.; Hukka, T. I.; Rantala, T. T. *Chem. Phys.*, in press.

(15) Perdew, J. P.; Chevary, J. A.; Vosko, S. H.; Jackson, K. A.; Pederson, M. R.; Singh, D. J.; Fiolhais, C. *Phys. Rev. B* **1992**, *46*, 6671.

(16) Perdew, J. P.; Burke, K.; Ernzerhof, M. *Phys. Rev. Lett.* **1996**, *77*, 3865.

(17) Slater, J. C. *Phys. Rev.* **1951**, *81*, 385.

(18) Dirac, P. A. M. *Proc. R. Soc. London* **1929**, *123*, 714.

(19) Vosko, S. H.; Wilk, L.; Nusair, M. *Can. J. Phys.* **1980**, *58*, 1200.

(20) Becke, A. D. *Phys. Rev. A* **1988**, *38*, 3098.

(21) Perdew, J. P. *Phys. Rev. B* **1986**, *33*, 8822.

(22) Lee, C.; Yang, W.; Parr, R. G. *Phys. Rev. B* **1988**, *37*, 785.

(23) Becke, A. D. *J. Chem. Phys.* **1993**, *98*, 5648.

(24) Schäfer, A.; Horn, H.; Ahlrichs, R. *J. Chem. Phys.* **1992**, *97*, 2571.

(25) Dunning, T. H., Jr. *Chem. Phys.* **1989**, *90*, 1007.

(26) Eichkorn, K.; Treutler, O.; Öhm, H.; Häser, M.; Ahlrichs, R. *Chem. Phys. Lett.* **1995**, *240*, 283.

(27) Seminario, J. M. *Recent Developments and Applications of Modern Density Functional Theory*; Elsevier: New York, 1996.

(28) Ahlrichs, R.; Bär, M.; Häser, M.; Kälmel, C. *Chem. Phys. Lett.* **1989**, *162*, 165.

(29) Koch, W.; Holthausen, M. C. *A Chemist's Guide to Density Functional Theory*; Wiley-VCH: New York, 2001.

(30) Ernzerhof, M.; Perdew, J. P.; Burke, K. *Density Functional Theory*; Nalewajski, R., Ed.; Spinger-Verlag: Berlin, 1996.

(31) Luo, C.; Guldi, D. M.; Imahori, H.; Tamaki, K.; Sakata, Y. *J. Am. Chem. Soc.* **2000**, *122*, 6535.

(32) Edwards, L.; Dolphin, D. H.; Gouterman, M.; Adler, A. D. *J. Mol. Spectrosc.* **1971**, *38*, 16.

(33) Canters, G. W.; Jansen, G.; Noort, M.; van der Waals, J. H. *J. Phys. Chem.* **1976**, *80*, 2253.